NASA TECHNICAL MEMORANDUM NASA TM - 76176

# RADIO ASTRONOMICAL SPACE SYSTEM OF APERTURE SYNTHESIS: FILLING OF THE SPATIAL FREQUENCY SPECTRUM

N. S. Kardashev, S. V. Pogregenko
and G. S. Tsarevskiy

Translation of "Radioastronomicheskaya Kosmicheskaya Sistema Aperturnogo Sinteza: Zapolneniye Spektra Prostranstvennykh Chastot", Academy of Sciences USSR, Institute of Space Research, Moscow, Report Pr-449, 1978, pp 1-50



(NASA-TM-76176) RADIO ASTRONOMICAL SPACE SYSTEM OF APERTURE SYNTHESIS: FILLING OF THE SPATIAL FREQUENCY SPECTRUM (National Aeronautics and Space Administration) 36 p HC A03/MF A01 CSCL 03A G3/89 N81-25887 Unclas 42219

NATIONAL AERONAUTICS AND SPACE ADMINSTRATION
WASHINGTON, D.C. 20546 JUNE 1980

STANDARD TITLE PAGE

| | | |
|---|---|---|
| 1. Report No. NASA TM-76176 | 2. Government Accession No. | 3. Recipient's Catalog No. |
| 4. Title and Subtitle RADIO ASTRONOMICAL SPACE SYSTEM OF APERTURE SYNTHESIS: FILLING OF THE SPATIAL FREQUENCY SPECTRUM | | 5. Report Date JUNE 1980 |
| | | 6. Performing Organization Code |
| 7. Author(s) N. S. Kardashev, S. V. Pogregenko and G. S. Tsarevskiy | | 8. Performing Organization Report No. |
| | | 10. Work Unit No. |
| 9. Performing Organization Name and Address SCITRAN Box 5456 Santa Barbara, CA 93108 | | 11. Contract or Grant No. NASW-3198 |
| | | 13. Type of Report and Period Covered Translation |
| 12. Sponsoring Agency Name and Address National Aeronautics and Space Administration Washington, D.C. 20546 | | 14. Sponsoring Agency Code |

15. Supplementary Notes Translation of "Radioastronomicheskaya Kosmicheskaya Sistema Aperturnogo Sinteza: Zapolneniye Spektra Prostranstvennykh Chastot", Academy of Sciences USSR, Institute of Space Research, Moscow, Report Pr-449, 1978, pp 1-50

16. Abstract

An examination is made of informational potentialities of radio astronomical space systems of aperture synthesis consisting of ground-based and space radio telescopes.

| | |
|---|---|
| 17. Key Words (Selected by Author(s)) | 18. Distribution Statement Unclassified - Unlimited |

| | | | |
|---|---|---|---|
| 19. Security Classif. (of this report) | 20. Security Classif. (of this page) | 21. No. of Pages | 22. |
| Unclassified | Unclassified | 36 | |



NASA-HQ

RADIO ASTRONOMICAL SPACE SYSTEM OF APERTURE SYNTHESIS: FILLING OF THE SPATIAL FREQUENCY SPECTRUM

By

N. S. Kardashev, S. V. Pogrebenko, G. S. Tsarevskiy

## Introduction

Recently more and more attention has been given to the development of long-range space radioastronomical systems (see [1,2] and references there, as well as [3,4]). Space radioastronomical systems afford the possibility of practically unlimited increase in the collecting areas of the antennas in combination with the possibility of synthesizing high frequency two-dimensional, and even three-dimensional [1] radio images with resolution that is inaccessible under ground conditions. /3*

In this respect, it is important to examine certain informational potentialities of the radio astronomical space system of aperture synthesis (abbreviation RASSAS) consisting of ground-based (GRT) and space (SRT) radio telescopes.

## 1. Statement of Task

One can demonstrate that the potentialities for the synthesis of radio images with RASSAS type systems are restricted by the sensitivity and resolution. As is known, the flux density from the source that has a brightness temperature of $T_B$ and solid angle $\Omega$ is

$$F = \frac{2kT_B}{\lambda^2}\Omega , \qquad (1)$$

*Numbers in margin indicate pagination in original foreign text.

where k--Boltzmann constant, $\lambda$--wavelength. The root-mean-square value of the maximum detected flux from a point source during observations on a two-antenna radio interferometer is /4

$$\sigma_F = \frac{\sqrt{2}\,kT}{A\cdot(\Delta\nu\cdot\Delta t)^{1/2}}, \qquad (2)$$

where T--temperature of system noises, A--effective antenna area ($A \approx \pi D^2/8$, $D = (D_1 x D_2)^{\frac{1}{2}}$, $D_1$ and $D_2$--diameters of interferometer antennas), $\Delta\nu$--width of band of received frequencies, $\Delta t$--integration time. After taking as $\Omega$ the solid angle $\pi(\lambda/B)^2/4$ of the resolution of an interferometer with base B, and considering that $P \geqslant \sigma_F$ we obtain

$$B \leqslant \left(\frac{T_B}{T}\right)^{1/2}\cdot(\Delta\nu\cdot\Delta t)^{1/4}\cdot D. \qquad (3)$$

In the case where the antenna temperature, governed by the source is greater than the noise temperature of the receivers (strong source), the inequality (3) becomes

$$B \leqslant \frac{\theta}{\theta_e}\left(\frac{F_e}{F}\right)^{1/2}\cdot(\Delta\nu\cdot\Delta t)^{1/4}\cdot D, \qquad (4)$$

where $\theta$, F--angular size and flux of entire source, $\theta_\theta$, $F_\theta$--angular size and flux of component in the synthesized image.

Assuming $\Delta\nu$=2 MHz, $\Delta t=10^3$ s, $T_B=10^{12}$ K (limit for synchrotron emission), T=10 K, D=30 m, $\theta$=100 ang. s, F=100 Yan (1 Yan=$10^{-26}$W $m^{-2}$ $Hz^{-1}$), we find that both for the weak and for the strong sources the limit base is about 2 million km. This indicates the outlook for the development of the RASSAS type systems that have the possibility of obtaining an extremely high angular resolution.

It is important to examine the possible beginning variant for the space radio astronomical system (we will call it RASSAS-1) that includes an SRT that orbits around the earth on a low ($H_o$=300-400 km) orbit. In light of the high relative rate of movement of the ground-based and space antennas of such a radio interferometer, a comparatively rapid filling of the spectrum of spatial frequencies is possible, and the diameter of the equivalent synthesizable aperture is on the order /5 of the earth's diameter. From the ratio between the maximum size of the base B, diameters of the antennas GRT and SRT $D_g$ and $D_s$, and the minimum detectable root-mean-square value of the brightness temperature in the image element $T_B$:

$$T_B = \frac{T B^2}{D_H D_K (\Delta\nu \cdot \Delta t)^{1/2}} \qquad (5)$$

we obtain for the values: $T=100$ K, $B=10^4$ km, $D_s=30$ m, $D_g=100$ m, $\Delta\nu=2$ MHz, $\Delta t=$ 1 day--the amount $T_B=10^7$ K. This means that the synthesis system with low-orbital SRT can be successfully employed to synthesize the images of compact sources of the type nuclei of galaxies, quasars, stars, etc. Practically all the known quasars and galactic nuclei (total number of several hundreds) have $T_B$ that surpass the indicated limit, while unambiguous radio images with resolution on the order of $10^{-3}$ ang. s, realized on interferometers with bases on the order of the earth's diameter, have been obtained only for several similar objects.

In the examined system, the antennas participate in a complex relative movement that generally speaking is aperiodical, which makes it possible to obtain a fairly complete spectrum of spatial frequencies; this significantly affects the unambiguity and quality of the obtained images [5,11]. A similar problem, in particular, is encountered in processing and interpreting the data obtained by the ground-based interferometers that are used for synthesis of the earth's rotation. /6 The latter are characterized by the elliptical shape of the motion tracks of the base vector projection in the plane of spatial frequencies (UV-plane) with a period of 12 hours [6]. Since during each subsequent period the track is repeated, then the percentage of filling of the UV-plane by the ground-based inteferometer that consists of a small number of antennas is very small (see below). In contrast to this, in RASSAS-1 practically complete and single-binding filling of the corresponding region of the UV-plane occurs; its boundaries are close to an ellipse.

In order to make a detailed study of the process of filling of the spatial frequency spectrum in the RASSAS-1 variant, and to compare the results of filling with the filling done by the ground-based systems of aperture synthesis consisting of two (type VLB) and many (type VLBA) antennas, a series of programs were compiled for numerical modeling (in Fortran IV language, realization on ES-1040 computer). Below is a brief description of the algorithms (section 2), results of the modeling and their discussion (section 3). A description and listings of the programs are given in the appendix.

## 2. Description of Modeling Algorithms

### 2.1. Coordinate System and Motion Equations

The movement of components in the system of aperture synthesis is examined in the following rectangular coordinate system OXYZ that is generally accepted both in the description of radio interferometers, as in the description of movement of artificial earth satellites: the center of the coordinate system "O" is located in the center of the earth, the axis "OZ" is directed towards the North Pole, the axis "OX"--towards the point of spring equinox, and the axis "OY" supplements the system of coordinates to the left set of three.

The motion equations of the ground-based radio telescopes in the adopted system of coordinates look like: /7

$$\vec{R}_H^{(i)}(t) = \begin{cases} x_H^{(i)}(t) = R_e \cos \varphi^{(i)} \cdot \cos(\Omega t + \lambda^{(i)} + \lambda_0), \\ y_H^{(i)}(t) = R_e \cos \varphi^{(i)} \cdot \sin(\Omega t + \lambda^{(i)} + \lambda_0), \\ z_H^{(i)}(t) = R_e \sin \varphi^{(i)}, \end{cases} \qquad (6)$$

where $R_e$--earth's radius, $\Omega$ --angular velocity of earth's rotation, $\varphi^{(i)}$, $\lambda^{(i)}$--geographical latitude and longitude of i-th GRT, $\lambda_0$--angle between the point of the spring equinox and the zero meridian at the beginning of the time reading.

The motion equations of the SRT on the assumption of a circular orbit and in the absence of precession and nutation of the orbit look like [7]:

$$\vec{R}_K(t) = \begin{cases} x_K(t) = R_0 [\cos(\omega t + \theta_0) \cos \Omega_0 - \cos i \sin(\omega t + \theta_0) \sin \Omega_0], \\ y_K(t) = R_0 [\cos(\omega t + \theta_0) \sin \Omega_0 + \cos i \sin(\omega t + \theta_0) \cos \Omega_0], \\ z_K(t) = R_0 \sin i \sin(\omega t + \theta_0), \end{cases} \qquad (7)$$

where $R_0$--radius of the SRT orbit, w--angular velocity of the SRT movement in the orbit, $\theta_0$--initial phase of movement of SRT, $\Omega_0$--longitude of ascending angle of orbit, i--angle of incline of orbital plane to plane of earth's equator.

Consideration for the effect of precession of the SRT orbital plane on the result of filling the UV-plane can be made by introducing the dependence of $\Omega_0$ on time although, as will be shown later, for duration of observation $T_0 \sim 1$ day one can not consider the precession.

The motion equations for the RASSAS-1 base looks like

$$\vec{B}_{HK}(t) = \vec{R}_K(t) - \vec{R}_H(t), \qquad (8)$$

while the motion equations of the base (i, j)-the pair of radio telescopes of the ground-based system of synthesis look like

$$\vec{B}_{HH}^{(i,j)} = \vec{R}_H^{(i)}(t) - \vec{R}_H^{(j)}(t). \qquad (9)$$

Sample geometry of the mutual arrangement and movement of the components in the RASSAS-1 system is presented in figure 1a. /8

2.2. Observed Object and Basis on UV-Plane

The position of the observed object in the celestial sphere is assigned by the coordinates $\alpha$ (direct ascent) and $\delta$ (inclination). The direction vector to the object $\vec{A}$ is defined as

$$A = \begin{cases} A_x = \cos\alpha \cdot \cos\delta, \\ A_y = \sin\alpha \cdot \cos\delta, \\ A_z = \sin\delta. \end{cases} \qquad (10)$$

The observation plane (spatial analog of the UV-plane) is assigned, like the plane passing through the center "0" of the coordinate system and perpendicular to the vector $\vec{A}$. The basis vectors on the observation plane, or what is the same with accuracy to scale, on the UV-plane, are selected as equal

$$\vec{B}_v = \begin{cases} B_{vx} = \cos\alpha \cdot \cos(\delta + \pi/2), \\ B_{vy} = \sin\alpha \cdot \cos(\delta + \pi/2), \\ B_{vz} = \sin(\delta + \pi/2), \end{cases} \qquad (11)$$

$$\vec{B}_u = [\vec{B}_v \times \vec{A}]. \qquad (12)$$

i. e., the vector $\vec{B}_v$ is formed from $\vec{A}$ by turning it 90° in the plane passing through $\vec{A}$ and the axis "OZ." The vectors $\vec{A}$, $\vec{B}_u$, $\vec{B}_v$ form an orthonormal basis; here the projection of the base vector in the system on $\vec{B}_v$ determines the resolution for the coordinate $\delta$ in the celestial sphere, the projection on $\vec{B}_u$--for the coordinate $\alpha$, while the projection for $\vec{A}$ is the difference in the signal course from the source to one of the radio telescopes in relation to the other. The plan for selecting the basis on the UV-plane is given in fig. 1b.

## 2.3. Calculation of Simultaneous Visibility of Object /9

For the GRT the condition of its visibility of the object corresponds to the fact that the radio telescope is located from the same side of the observation plane as the observed object, and for this the following condition must be fulfilled:

$$(\vec{R}_H^{(1)} \cdot \vec{A}) > 0 . \qquad (13)$$

For the SRT this condition must be supplemented, since depending on the height of its orbit the SRT will "see" the object in the space of a certain time after its switching to the side of the observation plane that is opposite in relation to the object until it enters the cylinder of shade created by the earth. Thus, the condition for cessation of the space radio telescope's visibility of the object can be written in the form

$$\left\{(\vec{R}_k \cdot \vec{A}) \leq 0\right\} \cap \left\{(\vec{R}_k \cdot \vec{B}_u)^2 + (\vec{R}_k \cdot \vec{B}_v)^2 - R_e^2 \leq 0\right\} . \qquad (14)$$

In the process of simulation the filling of a UV-plane by a pair of radio telescopes is interrupted if even one of them at the given moment is not in the condition to see the object.

## 2.4. Filling of the UV-plane

In the course of the modeling the values of the projections of the current base vector of the given pair of radio telescopes on the basis vectors $\vec{B}_u$ and $\vec{B}_v$ are determined. The obtained values are multiplied by the scale multiplier, selected such that the maximum base realizable by the system is written in the best manner into the discrete grid with assigned number of cells set aside for this. The projection values are rounded off to a whole number according to the /10
adopted quantization spacing. From the obtained whole-number projection values for the base vector on $\vec{B}_u$ and $\vec{B}_v$ the numbers of the cells are determined in the computer storage files that have been set aside for storage of the results. The model result of a single observation at the given base during the time corresponding to the adopted quantization spacing in time (in the given case, directly the quantization interval duration) is added to the contents of a cell thus determined, that is also symmetrical to it in relation to the center of the coordinates on the UV-plane. For a multiple-component system, this procedure is carried out in a cycle for all pairs of radio telescopes in the system. Thus, in the cells of the discrete presentation of the UV-plane the times for the stay of the system base projection in the corresponding areas of the continuous UV-plane

are summed.

The described procedure also provides for the possibility of obtaining charts for the filling of the UV-plane during multiple-frequency operation of the radio interferometer. The essence of the multiple-frequency filling consists of the fact that at the same time that a cell is filled that has coordinates $(u_I, v_I)$ on the UV-plane corresponding, say, to the first and the highest frequency of observation, cells are also filled with coordinates $(\eta_\ell u_I, \eta_\ell v_I)$, where $\eta_\ell = f_\ell / f_1 < 1$ is the $\ell$-th relative observation frequency. With the optimal selection of relative frequencies $\eta_\ell$ the filling of the UV-plane must be significant improved, of course, on the assumption that the distribution of radio **brightness** for the source remains unchanged in the entire range of observation frequencies. The UV-plane that is thus filled represents the sum of the filling in the first frequency, with the fillings obtained from it by the affine compression with the corresponding coefficients $\eta_\ell$.

Besides the increase in the number of filled cells on the UV-plane, the multiple-frequency operating pattern of the radio interferometer has an important /11
qualitative advantage over the traditional one-frequency pattern that consists of the possible determination of the phase of the visibility function from the differences in the interference signal phases for each frequency pair. We propose to examine this question in detail in another work.

## 2.5. Processing of the Modeling Results

The filling data obtained during the numerical modeling are further processed; the following are determined: value of the number of filled cells $N_f$, maximum base $B_{max}$ realized in the given numerical experiment, coefficient of time use (i.e., the relative portion of time during which simultaneous visibility of the studied object by both radio telescopes is realized), $K_t$. In addition, the function $\Phi(t_c)$ that is normed for a whole number of filled cells is determined; this is the function for the distribution of the number of filled cells according to the time of accumulation of $t_c$ on one cell.

In the analysis of the different interferometric systems, it is convenient to select their information content as the comparison parameter. The information content Sh according to Shennon is defined as

$$Sh = \sum_{ij} \ln[1 + (F/\sigma_F)_{ij}] \cdot \Delta u \cdot \Delta v , \qquad (15)$$

where $(F/\sigma_F)_{i,j}$ is the ratio signal/noise in the (i,j)-th cell of the discrete UV-plane, $\Delta u, \Delta v$--linear dimensions of the cell. With $F/\sigma_F < 1$ (weak source) one can be limited to the first term of the logarithm expansion into a Taylor series, and, taking into consideration that $F/\sigma_F \sim t_c^{\frac{1}{2}}$, we obtain

$$Sh_1 = \Delta u \cdot \Delta v \sum_{ij} t_c^{1/2}(u_i, v_j). \qquad (16)$$

In the case of a strong source, $F/\sigma_F \gg 1$, the logarithm in (15) can be /12
ignored as compared to the linear dependence of the information content on the number of filled cells. Thus, two estimates are possible for the relative information content of the interferometric systems: according to formula (16) for weak sources, and according to the number of filled cells for strong ones.

In this respect, during the processing of data from filling the UV-plane, we determined the coefficient of information content $Sh_I$ as well.

2.6. Block Diagram of Counting and Presentation of Results

The general block diagram of the procedure for numerical modeling of the process for filling the UV-plane is given below.

During the printing of the program the initial data are issued and the results of processing the data on filling of the UV-plane. The charts for filling /13
of the UV-plane are derived on the ADP (alphabet-digital printer) in two gradations: unfilled cells are represented by problems, filled--by the same symbol regardless of the time of accumulation on the given cell.

## 3. Results of Numerical Modeling and Their Discussion

### 3.1. Selection of Initial Parameters

A system was selected as the model for RASSAS-1 that consists of one GRT that has the geographical coordinates of

latitude $\varphi = 45°$

longitude $\lambda = 0°$,

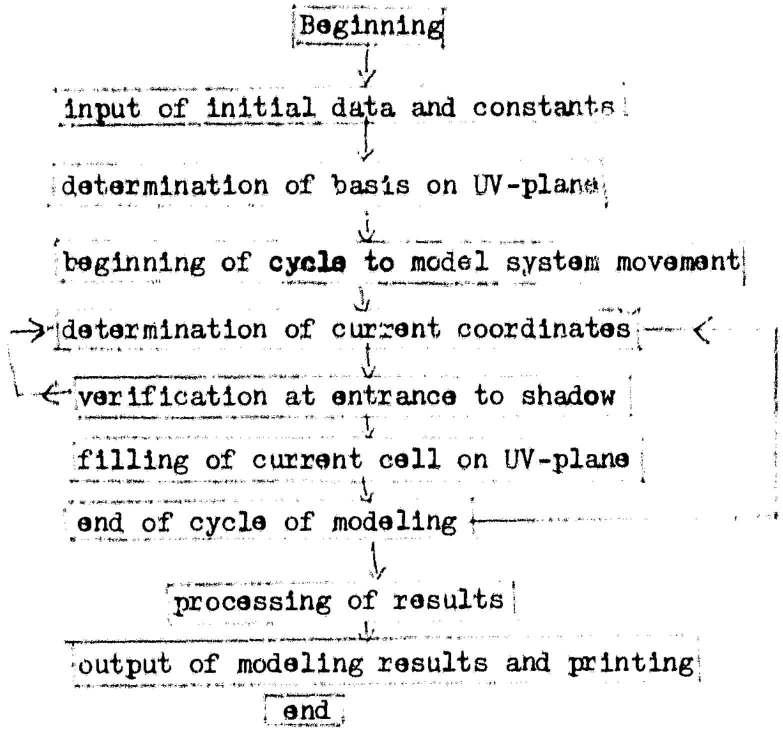


and one SRT that rotates around the earth on a circular orbit with the following parameters:

altitude of orbit $H_0 = 350$ km,
period of revolution $T_0 = 92$ min,
incline of orbital plane $i = 52°$,
longitude of ascending loop $\Omega_0 = 0°$,
beginning phase $\theta_0 = 0°$

The geometry of the system is presented in figure 1a.

It is evident that if the duration of the observation period $T_H \gg T_0$, then the dependence of the resulting filling of the UV-plane on $\theta_0$ will be weak. With $T_H \geq 24$ hours the dependence on $\lambda$ will also be weak. For this reason, the zero values of these parameters were selected purely formally. As will be shown below, the dependence on $\Omega_0$ is manifest as the dependence on the difference of $\alpha - \Omega_0$, where $\alpha$ is the direct ascent of the observed object. In this respect, variations /14
were not made in the value $\Omega_0$. The values $i$ and $H_0$ were selected close to the corresponding values of the orbit of the "Salyut" station. During the numerical modeling calculations were made for the situations that are distinguished by the

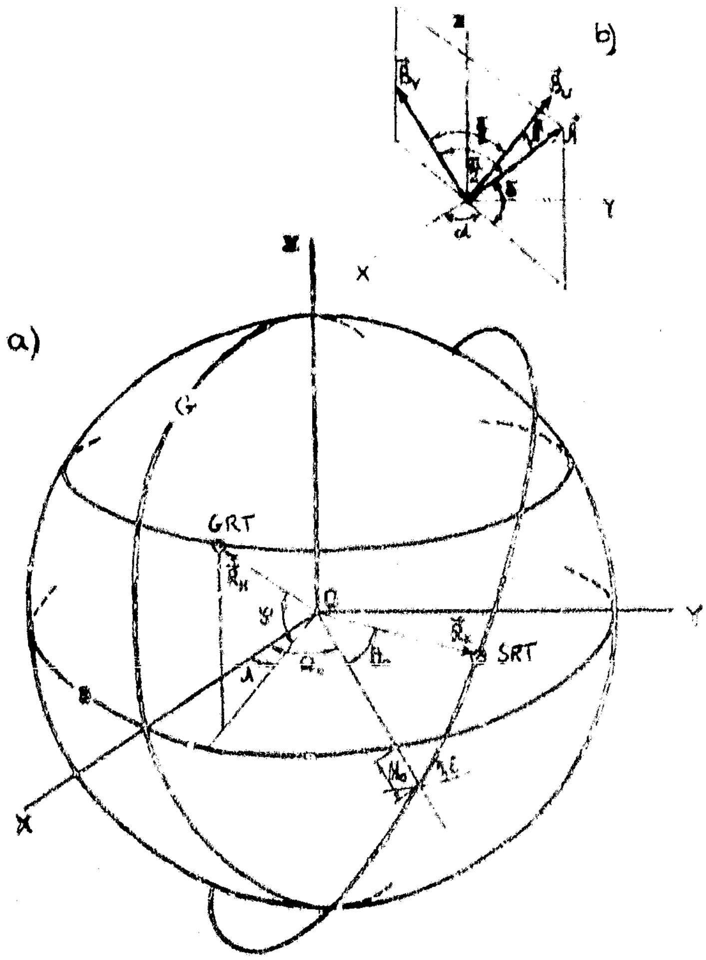


Figure 1. Geometry of Radio Astronomical Space System of Aperture Synthesis (RASSAS-1)
a) mutual arrangement of the ground-based (GRT) and space (SRT) radio telescopes (E--earth's equator, G--Greenwich meridian); b) plan for selecting basis on UV-plane

position of the observed object in the celestial sphere and the duration of the observation period, as well as by the number of analyzable frequencies during multiple-frequency filling of the UV-plane. Here, practically always, with the exception of the case where the spatial response of the system was computed, the UV-plane was presented in the form of a mass of 101 x 101 cells; here the cell with the number (51,51) corresponds to the center of the coordinates on the UV-plane, i.e., in our illustrations for clearness both halves of the UV-plane are presented. The linear size $\Delta R$ of one cell is selected from the correlation

$$50\,\Delta R = 2R_0 ,\qquad (17)$$

where $R_0$--radius of the SRT orbit, which corresponds to the fact that the maximum base realizable by the system equalling $\approx 2R_0$ will have a magnitude of 50 cells in the discrete presentation. The spacing $\Delta t$ of the quantization of the process in time is selected as equal to 6 seconds, which corresponds roughly to 1/4 + 1/10 of the average time that the projection of the system base vector stays in one cell of the UV-plane during a single passage through it.

### 3.2. Dynamics of the Process of UV-Plane Filling

Figures 2 and 3 present maps of filling for the UV-plane in the RASSAS-1 system that were computed without consideration for the precession of the SRT orbit for the observed objects with coordinates $\alpha=0^h$, $\delta=45°$ (fig. 2) and $\alpha=18^h$, $\delta=45°$ (fig. 3) with different durations of the observation period $T_H$. The numbers /15 in the left upper angles of the charts presented here correspond to the complete duration of the observation as follows

| No | 1 | 2 | 3 | 4 | 5 | 6 | 7 | 8 |
|---|---|---|---|---|---|---|---|---|
| $T_H$ (hour) | 1.5 | 3 | 6 | 12 | 24 | 48 | 96 | 192 |

On the charts corresponding to the short ($T_H \leq 12$ hours) periods of observation, the interruptions in the movement tracks of the projection for the system base vector on the UV-plane are clearly seen; they are due to the entrance of the SRT into the earth's shadow and the movement of the GRT during the time that the SRT is in the shadow, as well as the general epicycloid nature of the filling.

Figure 4 presents graphs for the dependence of the number $N_f$ of filled cells (in thousands) on the duration of the filling period $T_H$. The solid line represents the dependence for the source with coordinates $\alpha=0^h$, $\delta=45°$, and the dotted line--for the source with $\alpha=18^h$, $\delta=45°$. It is apparent that, with the given quantization of the UV-plane the filling occurs fairly intensively all the way to time $T_H$= 4 days, and then becomes saturated, which is induced by the repeated entrance of the projection of the system base vector into the previously filled cells. Here the coefficient of filling a single-communications region that contains all the filled cells is fairly high, and is 0.5-0.8. It is natural that the

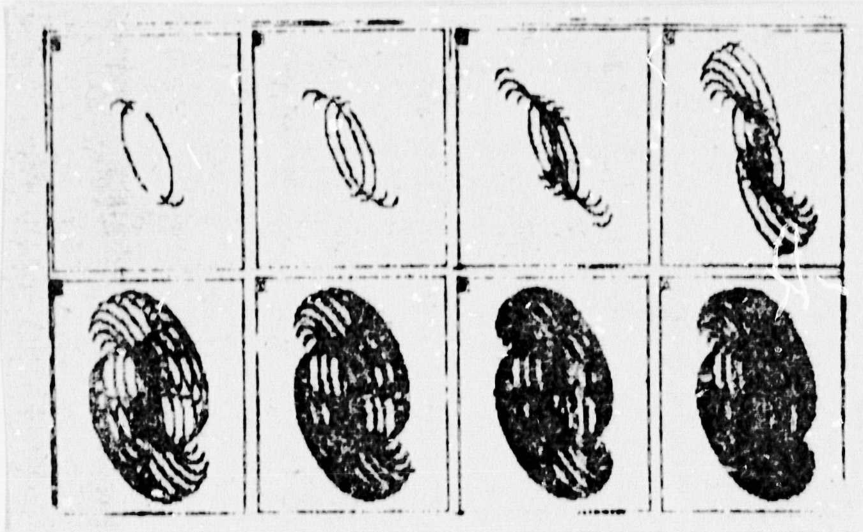

Figure 2. Charts for Filling the UV-plane of the RASSAS-1 System with: $\varphi = 45°$, $\lambda=0°$, $H_0=350$ km, $T_0=92$ min, $i=52°$, $\Omega_0=0°$, $\theta_0=0°$, $\alpha=0^h$, $\delta=45°$ for the filling time $T_H$: 1.5 h (1), 3 h (2), 6 h (3), 12 h (4), 24 h (5), 48 h (6), 96 h (7), 192 h (8). The UV-plane is divided into 101x101 cells.

reduction in the linear dimensions of the cell, or what is the same, the increase in their number in the discrete presentation of the UV-plane will reduce the coefficient of filling, and will shift the moment that the filling process becomes saturated toward the greater times.

Precession significantly alters the dynamics of UV-plane filling, but only at long observation durations. Thus, with rate of precession 1-2 deg/day, the linear changes in the base vector with characteristic size $R_0=6700$ km will be 200-400 km in 2 days time, which corresponds to 1-2 cells with the given quantization. Precession will reduce the degree of covering of the newly filled cells in the peripheral region of the UV-plane, and correspondingly will increase their number, and, what is important from the viewpoint of the tasks to be solved by the system, on large values of the base. With $T_H \sim 1$ day, the effect of precession cannot have a significant effect on the filling.

The graph presented in figure 5 (solid line and dotted line correspond to the same positions of the observed object as in fig. 4) for the dependence of the average time of accumulation on one cell $t_{av}$ on the duration of the observation period $T_H$ also indicates the effect of repeated entrance of the base vector projection into previously filled cells, and namely: up to time $T_H \approx 2$ days $t_{av}$

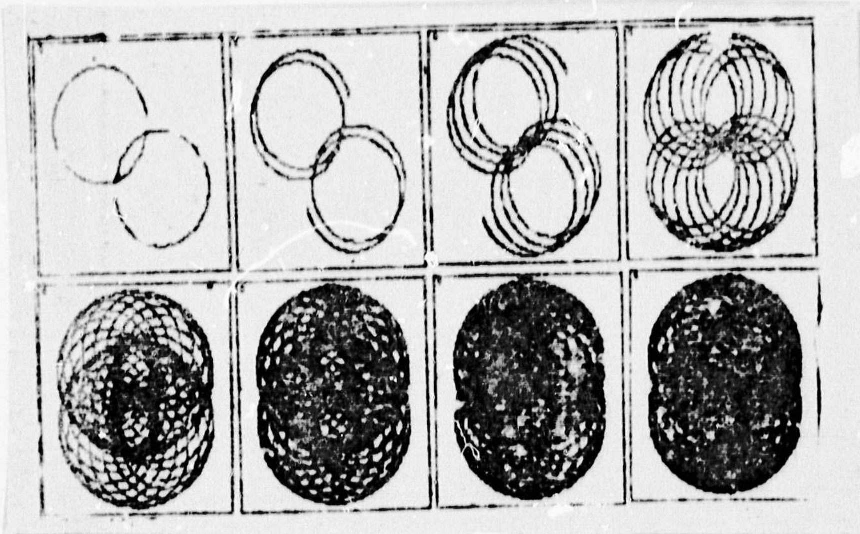

Figure 3. Chart of UV-Plane Filling by the System RASSAS-1 with: $\vartheta=45°$, $\lambda=0°$, $H_o=350$ km, $T_o=92$ min, $i=52°$, $\Omega_o=0°$, $\theta_o=0°$, $\alpha=18^h$, $\delta=45°$ for the filling time $T_H$: 1.5 h (1), 3 h (2), 6 h (3), 12 h (4), 24 h (5), 48 h (6), 96 h (7), 192 h (8). The UV-plane is divided into 101x101 cells.

practically is not altered, which indicates the low percentage of repeated entrances, and then begins to increase rapidly (practically linearly with $T_H$). The effect of precession of the SRT orbital plane must slow this growth down at long observation times.

### 3.3. Dependence of UV-Plane Filling on Coordinates of the Observed Object

The data presented in figures 2-5 indicate the significant change in the results of filling depending on the coordinates (in the given case--on direct ascent) of the studied object. Thus, for the source with $\alpha=18^h$, $\delta=45°$, the number of cells filled in 24 h with other conditions equal, is roughly two times greater than for the source with $\alpha=0^h$ and the same incline. This is linked to the fact that with different coordinates, the source "sees" the plane of the SRT orbit at different angles. The optimal from the viewpoint of the completeness of filling the UV-plane will be that mutual arrangement of the studied object and the SRT orbital plane, where the vector $\vec{A}$ of direction to the object will be perpendicular /17
to the orbital plane; in other words, when the orbital plane will coincide with the observation plane. If one searches for the extreme only for $\alpha$ with the remaining parameters fixed, then it will be reached with $\alpha^{(m)}=\Omega_o-\pi/2$ for $i\leq\pi/2$ and $\alpha^{(m)}=\Omega_o+\pi/2$ for $\pi/2< i < \pi$, where $\alpha^{(m)}$ is expressed in radians. Due to the influence of both the SRT and GRT entering the shadow, and depending on $\vartheta$ and $\lambda$, the value $\alpha^{(m)}$ that gives the maximum number of filled cells on the UV-plane for

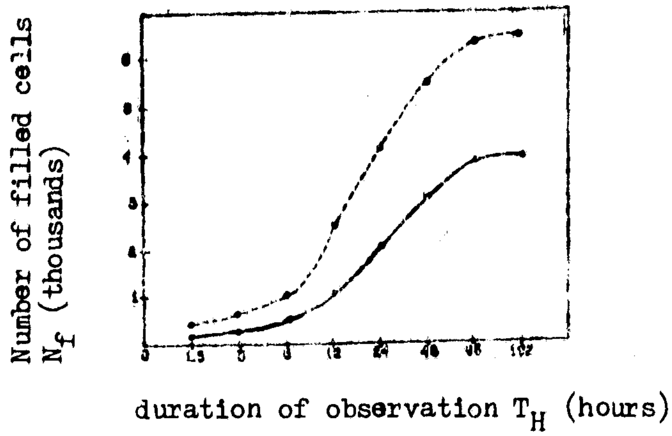


Figure 4. Dependence of Number $N_f$ (in thousands) of Filled Cells on UV-Plane on Duration of Filling $T_H$ with: $\varphi=45°$, $\lambda=0°$, $H_0=350$ km, $T_0=92$ min, $i=52°$, $\Omega_0=0°$, $\theta_0=0°$, $\delta=45°$, $\alpha=18^h$ (dotted line) $\alpha=0^h$ (solid line) with division of the UV-plane into 101 x 101 cells.

the orbit with fixed parameters can be somewhat altered in relation to the value determined above.

Figure 6 presents the charts for filling the UV-plane in 24 h for the objects with $\alpha=0^h$ and $\delta$ linked to the number of the chart as follows:

| No. | 1 | 2 | 3 | 4 | 5 | 6 | 7 | 8 |
|---|---|---|---|---|---|---|---|---|
| δ | 0° | 13° | 26° | 39° | 51° | 64° | 77° | 90° |

and figure 7--the charts for filling the UV-plane in 24 h for objects with $\delta=45°$ and $\alpha$ linked to the number of the chart as follows:

| No | 1 | 2 | 3 | 4 | 5 | 6 | 7 | 8 |
|---|---|---|---|---|---|---|---|---|
| α | $0^h$ | $3^h$ | $6^h$ | $9^h$ | $12^h$ | $15^h$ | $18^h$ | $21^h$ |

The graph presented in figure 8a shows the dependence of the number of filled cells on the UV-plane (in thousands) on the incline of the studied object with $\alpha=0^h$ (solid line) and $\alpha=18^h$ (dotted line), $T_H=24$ h, and figure 8 b--the dependence of the number of filled cells on $\alpha$ of the studied object with $\delta=45°$ and other conditions equal. On figure 8b, the maximum with $\alpha=18^h$ is clearly visible, which precisely corresponds to the case where the source with fixed $\delta$ "sees" the plane /18
of the orbit at the maximum angle.

This fact has great importance for selecting the sequence of observation of

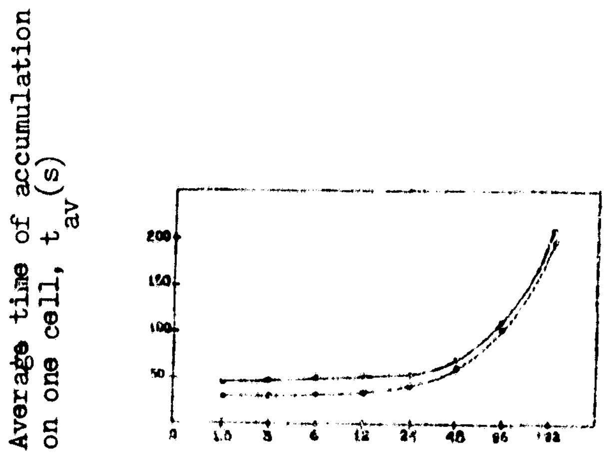


duration of observation $T_H$(hours)

Figure 5. Dependence of Average Time of Accumulation on One Cell $t_{av}$ on the Duration of Filling $T_H$ for:
$\vartheta=45°$, $\lambda=0°$, $H_o=350$ km, $T_o=92$ min, $i=52°$, $\Omega_o=0°$, $\theta_o=0°$, $\delta=45°$, $\alpha=0^h$ (solid line) and $\alpha=18^h$ (dotted line) with division of the UV-plane into 101 x 101 cells.

several objects, since the presence of precession of the orbital plane in principle can permit the selection for each object of that moment of the beginning of observations $t_o$, where the filling of the UV-plane will be the maximum possible for it, which will permit an increase in the efficiency of the observation process.

The optimal moment for the beginning of the observations of the assigned object can be defined from the correlation

$$\Omega_o(t_o) - \pi/2 = \alpha . \qquad (18)$$

The value $t_o$ can be determined with accuracy up to several days, for during such a period the effect of orbital precession on the process of filling the UV-plane is insignificant.

If one observes the source not only with the optimal value of the direct ascent, but also with the optimal value of incline $\delta_o$, then besides the maximum filling of the spectrum of spatial frequencies, the minimum frequency of interference of the signals will occur. In fact, in this case the projection of the rate of SRT movement on the vector $\vec{A}$ of direction to the object will equal zero, and consequently the change in the geometric delay (from here the interference frequency follows) will be determined only by the rate of movement of the ground-based telescope.

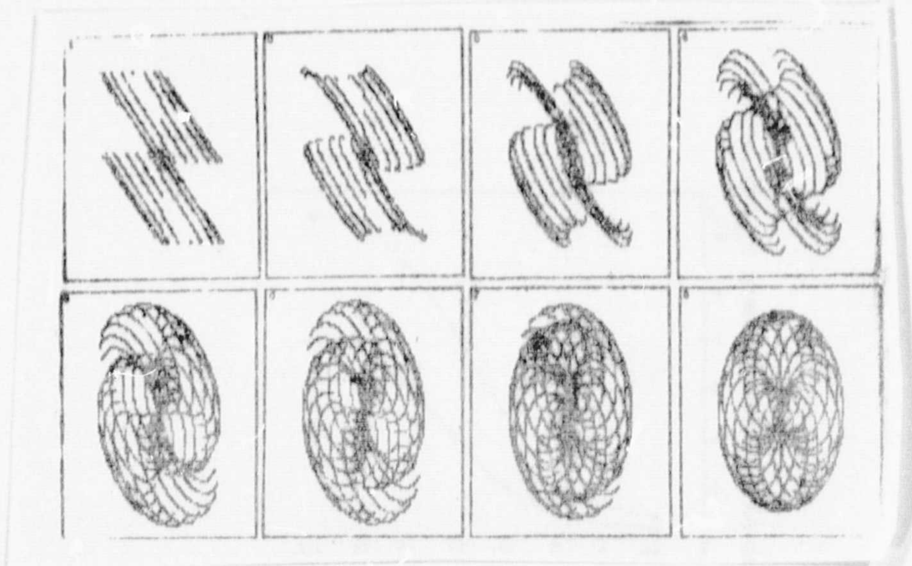

Figure 6. Maps of Filling the UV-Plane by the System RASSAS-1 with: $T_H$=24 h, $\varphi$=45°, λ=0°, H =350 km, $T_0$ =92 min, i=52°, Ω =0°, $\theta_H$=0°, δ=45° and different α: $0^\circ$(1), $13^\circ$(2), $26^\circ$(3), $39^\circ$(4), $51^\circ$(5), $64^\circ$(6), $77^\circ$(7), $90^\circ$(8). The UV-plane is divided into 101 x 101 cells.

In practice a certain range of angles for the incline will exist, in which the projection of the SRT velocity on the vector $\vec{A}$ will be fairly small, for example, it will not exceed the relative rate of movement of the radio telescopes in the VLBI type system with basis equal to the earth's diameter. We will introduce into the examination the amount of deviation $\Delta\delta$ of incline from the optimal value: /19
$\Delta\delta = \delta - \delta_0$. Then the maximum value of the velocity projection of the SRT on the vector $\vec{A}$ can be estimated by the amount

$$U_{II}(KPT) = \omega R_0 |\sin\Delta\delta| = \frac{2\pi R_0}{T_0}|\sin\Delta\delta| . \qquad (19)$$

Correspondingly, the maximum value for the projection of the relative rate of movement of the radio telescopes in the VLBI system will be

$$U_{II}(VLBI) = 2R_e\Omega = \frac{4\pi R_e}{T_e}, \qquad (20)$$

where $T_e$=24 h. Thus, one can estimate the range of angles at which $V_{II}(SRT) \le V_{II}(VLBI)$ from the correlation

$$\frac{2\pi R_0}{T_0}|\sin\Delta\delta| \le \frac{4\pi R_e}{T_e}, \qquad (21)$$

which yields

$$|\sin\Delta\delta| \le \frac{2T_0}{T_e} \simeq 0.125$$

or

$$-7^\circ \leq \Delta\delta \leq 7^\circ$$

That is, with the optimal α in the range of inclinations ($\delta_0$-7°, $\delta_0$+7°) the frequency of interference for RASSAS-1 will not be greater than during observations on the VLBI with base close to the earth's diameter. Consequently, in this case the requirements for the fast-response and the range of indefiniteness selection for the Doppler shift in frequency during observations on RASSAS-1 will be the same as for the ground-based system. In addition, an important consequence of selecting the optimal mutual orientation of the studied source and the orbital plane of the SRT is that the errors in determining the coordinates and velocity of the SRT, that are mainly linked to indefiniteness of its position along the orbit enter the analysis of the weight factor sin Δδ, i.e., their influence will be significantly reduced.

The value of the pure time synthesis is important from the viewpoint of /20
efficient observations, i.e., that part of the complete observation time during which simultaneous visibility of the studied source by both radio telescopes in the system was realized. Figure 9 presents the dependence of the pure time synthesis $T_c$ on the coordinate α of the studied object with δ=45° and complete observation time $T_H$=24 h. It is apparent that with the value $\alpha=18^h$ that is the optimal from the viewpoint of the complete filling of the UV-plane, the maximum pure synthesis time is also realized.

## 3.4. Distribution of the Number of Filled Cells of the UV-plane According to the Accumulation Time

With the adopted algorithm for filling the cells of the UV-plane, the accumulation times for one cell are distinguished among themselves, which is linked, first of all, to the nonuniformity in the rate of movement of the projection for the system base vector over the UV-plane and secondly, to the repeated entrances of the base vector projection into the already filled cells, which occurs most often with small values of the current base. The range of change in time of accumulation for one cell is 2-3 orders for one realization of filling; however, such a broad range is mainly due to the presence of cells with very large accumulation time; as a rule there are few of these (units).

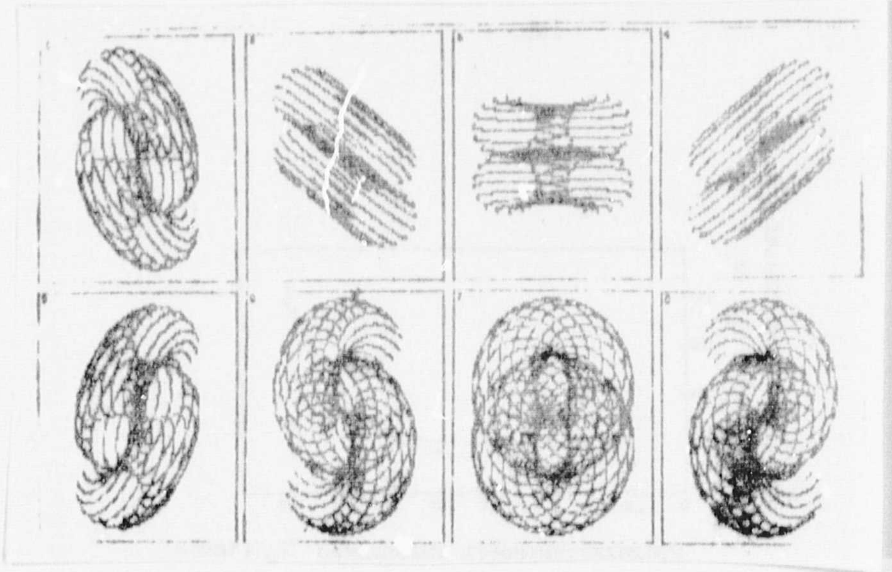

Figure 7. Charts for Filling UV-Plane of RASSAS-1 System with: $T_H$=24 h, $\varphi$=45°, $\lambda$=0°, $H_0$=350 km, $T_0$=92 min, i=52°, $\Omega_0$=0°, $\theta_0$=0°, $\delta$=45° and different $\alpha$: $0^h$ (1), $3^h$(2), $6^h$(3), $9^h$(4), $12^h$ (5), $15^h$ (6), $18^h$(7), $21^h$ (8). The UV-plane is divided into 101 x 101 cells.

The graphs presented in fig. 10a, b show the functions $\Phi(t_c)$ for the distribution of the number of filled cells according to accumulation time on one cell $t_c$, obtained for $T_H$=24 h, with coordinates of the studied object $\alpha=18^h$, $\delta$=45°, and division of the UV-plane into 101 x 101 (fig. 10a) and 128 x 128 (fig. 10b) cells. The maximum values of $t_c$ plotted on the horizontal axes of the given /21 graphs correspond to the maximum values for the accumulation time for one cell that were realized during the given numerical experiments. Both graphs have clearly pronounced maximums at accumulation times close to the average time of accumulation $t_{av}$ shown on the graphs by a vertical line. It is apparent that with an increase in the number of cells in the discrete presentation of the UV-plane the maximum of the distribution function appears more distinctly. The percentage of points with accumulation time lower than 0.5 $t_{av}$ in both cases is small (≈10%), and is reduced with an increase in the number of cells in the division of the UV-plane.

It is worth noting that the cells with large accumulation time can be used for the purpose of calibrating the system and for accurate phase correlation in solving the tasks of radio astrometry.

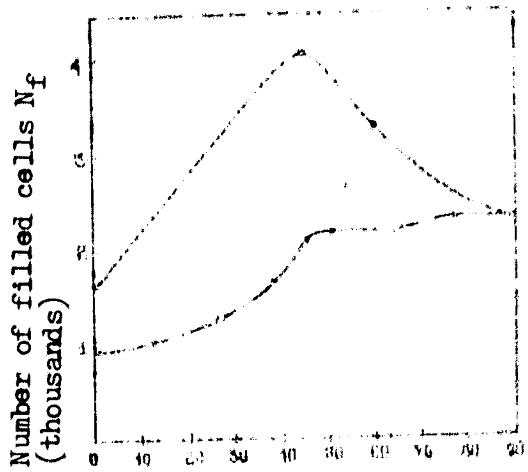


Inclination δ(°)

a

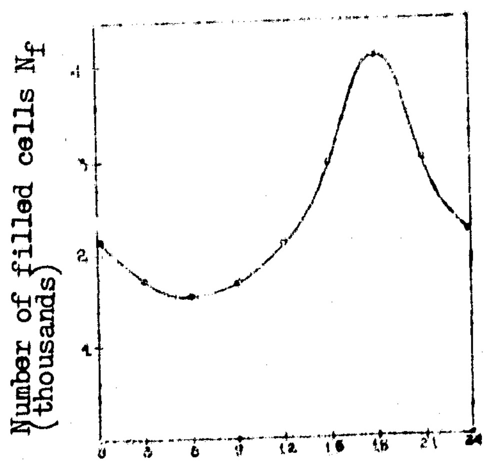


direct ascent α (n)

b

Figure 8. Dependence of Number of Filled Cells $N_f$ (in thousands) on UV-Plane on Inclination δ of Studied Object for: $\alpha=0^h$ (solid line), and $\alpha=18^h$ (dotted line) with $T_H= 24$ h, $\vartheta=45°$, $\lambda=0°$, $H_o=350$ km, $T_o=92$ min, $i=52°$, $\Omega_o=0°$, $\theta=0°$. The UV-plane is divided into 101 x 101 cells.

b. Dependence of Number of Filled Cells $N_f$ (in thousands) on UV-plane on Direct Ascent of α of Studied Object with $\delta=45°$ and the other conditions the same as in fig. 8a.

## 3.5. Multiple-Frequency Filling of the UV-Plane

Figure 11 presents charts for filling of the UV-plane in 24 h for the source with $\alpha=18^h$, $\delta=45°$ with one-, two-, three- and four-frequency filling with relative frequencies 1.0, 0.9, 0.8 and 0.7, and figure 12 shows the dependence of the number of filled cells on the number of filling frequencies for the sources with $\alpha=0^h$, $\delta=45°$ (solid line) and $\alpha=18^h$, $\delta=45°$ (dotted line). The values that are discrete in their essence, presented in fig. 12, are connected by a smooth curve for clarity.

On figure 12, one can see the significant growth in the number of filled cells during the transition from one frequency to two, and the saturation in the growth during further increase in the number of frequencies. However, with varying spacing of the difference in relative frequencies, different stages in the filling increase are possible. In particular, the charts presented in figure 11 show the possible additional increase in the number of filled cells during the /22 introduction of yet another frequency, closer to 1.0 than 0.9, since this would permit the filling of the gaps present in the peripheral regions of the examined charts; the more so since this gives the advantage to the number of cells that have high values of spatial frequencies.

## 3.6. Spatial Response of the RASSAS-1 System

The spatial response (beam pattern of the synthesized aperture) in the RASSAS-1 system was obtained by a Fourier transform of the UV-plane filling obtained during modeling of the observation of a source with $\alpha=18^h$, $\delta=45°$, $T_H=$ 24 h, and with the division of the UV-plane into 128 x 128 cells.

The obtained response, constructed in the form of a relief map, is presented in figure 13. The maximum lateral lobe of the given response is 12% of the magnitude of the central maximum, while the root-mean-square level of the lateral lobes equals 1.2%. The maximum and the root-mean-square levels of the lateral lobes can be significantly reduced, both with an increase in the duration of the observation $T_H$ above 24 h, and with the use of the extant methods of image clarification [8, 9].

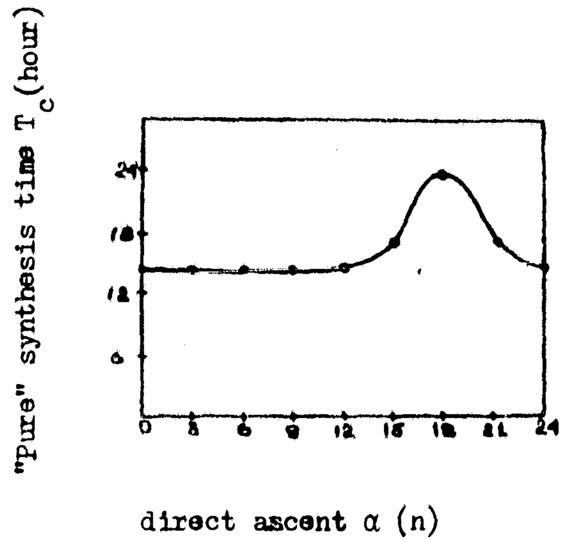


Figure 9. Dependence of Pure Synthesis Time $T_c$ in RASSAS-1 System on Direct Ascent α of Studied Object with: $T_H$=24 h, $\varphi$=45°, λ=0°, $H_0$=350 km, $T_0$=92 min, i=52°, $\Omega_0$=0°, θ=0°, δ=45°

## 3.7. Comparison with the Ground-Based Systems Type VLBI and VLBA

To compare the filling of the UV-plane by the RASSAS-1 system with the filling by the created ground-based systems of aperture synthesis using the earth's rotation, two systems were selected of radio interferometers: a) two-component VLBI with antennas that have the following geographical coordinates:

| No of antenna | latitude | longitude |
|---|---|---|
| 1 | 42.0° | -80.0° |
| 2 | 44.5° | 34.0° |

/23

which roughly corresponds to the interferometer Simeyz-Khaystek; b) the VLBA system suggested in [10], consisting of 10 radio telescopes whose geographical coordinates are given below

| No. of antenna | Latitude | Longitude |
|---|---|---|
| I | 40.4° | - 3.2° |
| 2 | 38.4° | - 77.2° |
| 3 | 38.5° | - 79.8° |
| 4 | 38.5° | - 81.5° |
| 5 | 38.5° | - 85.5° |

| | | |
|---|---|---|
| 6 | 38.5° | − 88.0° |
| 7 | 38.5° | − 99.5° |
| 8 | 38.5° | 111.0° |
| 9 | 38.5° | −122.4° |
| 10 | 19.8° | −155.5° |

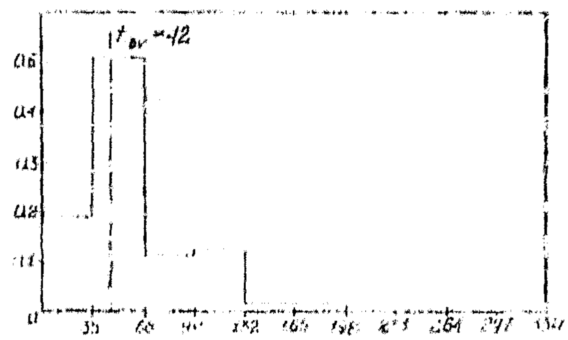

accumulation time for one cell $t_c$ (s)

a

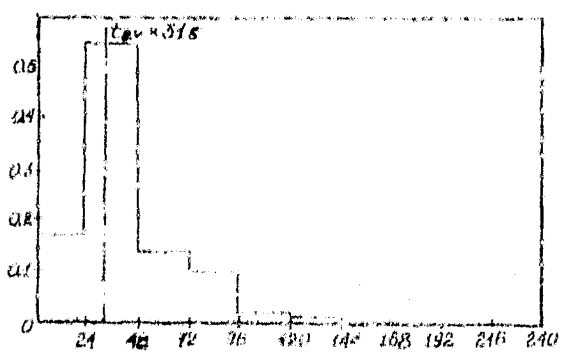

accumulation time for one cell $t_c$ (s)

b

Figure 10. Distribution $\Phi t_c$ of Number of Filled Cells on UV-plane according to Accumulation Time for One Cell $t_c$ with: $T_H$=24 h, $\vartheta$=45°, $\lambda$=0°, $H_o$=350 km, $T_o^c$=92 min, i=52°, $\Omega_o$=0°, $\theta_o$=0°, $\alpha=18^h$, $\delta$=45°, and with division of the UV-plane into: a) 101 x 101 cells, b) 128 x 128 cells.

Figure 11. Charts for Filling the UV-Plane by the RASSAS-1 System with Multiple-Frequency Filling with Relative Frequencies: $\eta_\ell$ = 1.0, 0.9, 0.8 and 0.7 with $T_H$=24 h, $\gamma$=45°, $\lambda$=0°, $H_o$=350 km, $T_o$=92 min, i=52°, $\Omega_o$=0°, $\theta_o$=0°, $\alpha=18^h$, $\delta$=45°, division of the UV-plane into 101 x 101 cells and with varying number of frequencies n=1,2,3,4.

It was considered in the calculations that the dimensions of all the antennas in the systems RASSAS-1, VLBI and VLBA were the same. The scales of the charts for the UV-plane for the VLBI and VLBA systems were selected from the correlations:

$$60 \cdot \Delta R_{VLBI} = 2 R_e,$$
$$50 \cdot \Delta R_{VLBA} = 2 R_e$$

in order to reduce the values for the maximum bases realizable by this system, expressed in the number of UV-plane cells, to the values realizable by the RASSAS-1 system. The obtained values $\Delta R$ are 212 km for VLBI and 256 km for VLBA, which is close to $\Delta R$=272 km for RASSAS-1, therefore the charts for filling of the UV-plane and their statistical characteristics obtained for different systems can be directly compared among themselves by taking into consideration the fact /24
that the number of antennas participating in the VLBA operation is considerably greater than the number of antennas in the RASSAS-1 system and the VLBI system.

Figure 14 presents the charts for filling of the UV-plane by the VLBI model system for objects with $\delta$ corresponding to the chart number as follows:

| No | 1 | 2 | 3 | 4 | 5 | 6 |
|---|---|---|---|---|---|---|
| $\delta$ | 0° | 15° | 30° | 45° | 60° | 90° |

Figure 15 presents charts for the filling of the UV-plane by the VLBA systems (index "G"--ground-based at the chart number) and RASSAS-1 (index "S"--

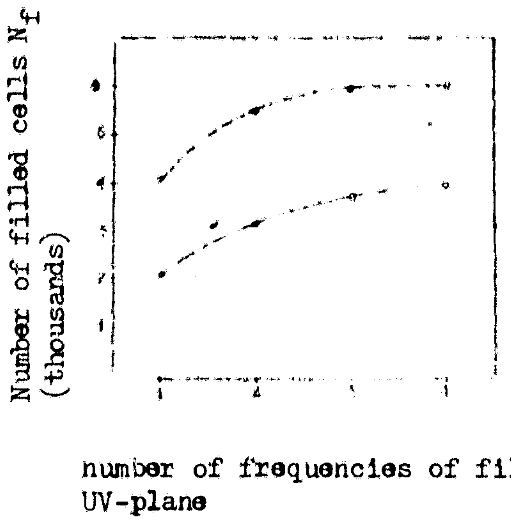


Figure 12. Dependence of Number of Filled Cells $N_f$ (in thousands) on UV-Plane with Multiple-Frequency Filling on Number of Simultaneously Analyzable Frequencies with Relative Frequencies: $\eta_\ell$=1.0, 0.9, 0.8, 0.7 and $T_H$=24 h, $\varphi$=45°, λ=0°, $H_o$=350 min, $T_o$=92 min, i=52°, $\Omega_o$=0°, $\theta_o$=0°, δ=45°, α=$0^h$ (solid line) and α=$18^h$ (dotted line).
UV-plane divided into 101 x 101 cells.

space)for objects with inclination corresponding to the chart number as follows:

| No | 1 | 2 | 3 | 4 |
|---|---|---|---|---|
| δ | 0° | 45° | 60° | 90° |

For the interferometric systems type VLBI and VLBA the value of the direct ascent of the studied source with daily synthesis is quite insignificant, and for the RASSAS-1 in the given numerical experiments α was selected as equal to 18.

For comparison of the results of filling the UV-plane by the model systems VLBI, VLBA and RASSAS-1, the table presents the values for the number of filled cells $N_f$, the relative information content for a weak signal $Sh_I$, and the maximum base $B_{max}$ realizable in the given numerical experiment. The complete observation time in each case equals 24 h. The table corresponds to the situations whose charts are presented in fig. 14 and fig. 15.

Conclusions

The calculations presented above, in particular, the charts for the

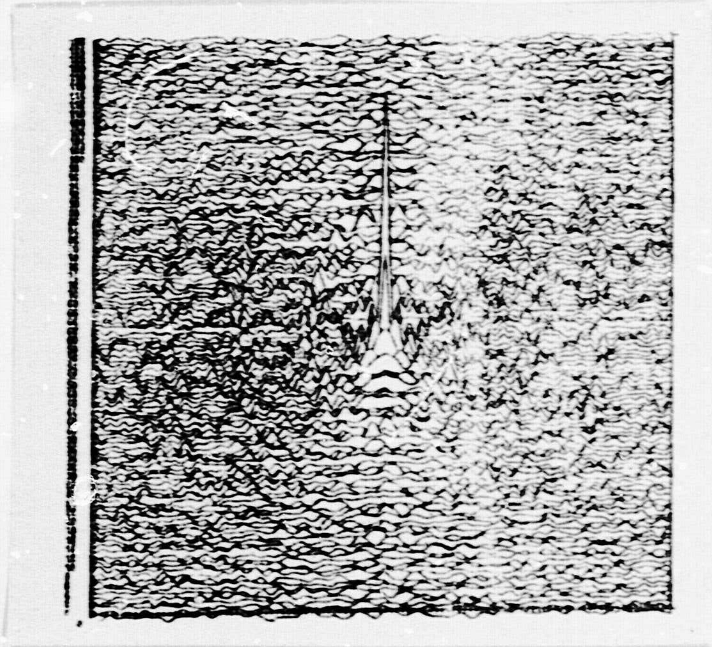

Figure 13. Beam Pattern of Synthesized Aperture System RASSAS-1 with :
$T_H=24$ h, $\varphi=45°$, $\lambda=0°$, $H_o=350$ km, $i=52°$, $\Omega_o=0°$, $\theta=0°$, $\alpha=18^h$, $\delta=45°$, division of the UV-plane into 128 x 128 cells.

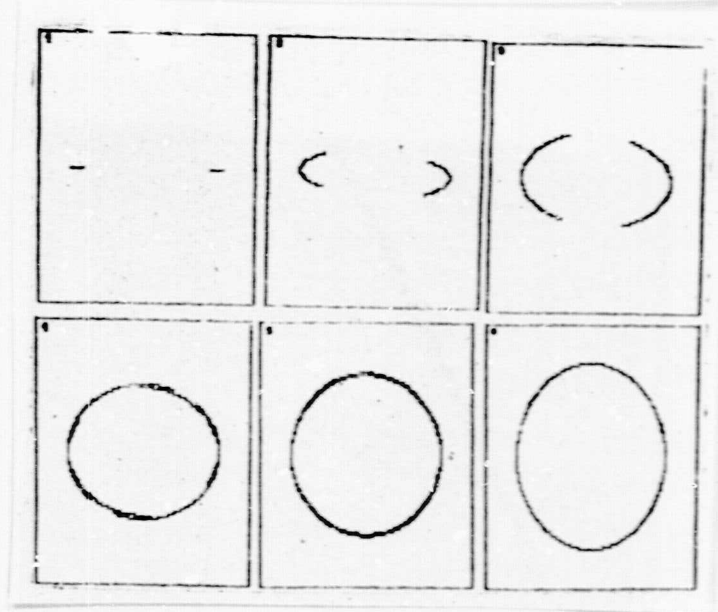

Figure 14. Charts for Filling of UV-Plane by System VLBI with:
$T_H=24$ h, $\varphi_I=42.0°$, $\varphi_2=44.5°$, $\lambda_I=-80.0°$, $\lambda_2=34.0°$ for the studied objects with $\delta=0°$(1), 15° (2), 30° (3), 45° (4), 60° (5), 90° (6).
Division of the UV-plane into 101 x 101 cells

| δ | parameter | system: VLBI 2 telescopes | VLBA 10 telescopes | RASSAS-1 2 telescopes |
|---|---|---|---|---|
| 0° | $N_\xi$ | I4 | I29 | I 586 |
| | $Sh_I$ | $2.8 \cdot I0^{7}$ | $I.0 \cdot I0^{I0}$ | $6.6 \cdot I0^{9}$ |
| | $B_{max}$ (км) | 7 650 | I0 600 | I2 450 |
| 45° | $N_\xi$ | 334 | 2 267 | 4 099 |
| | $Sh_I$ | $2.9 \cdot I0^{8}$ | $5.4 \cdot I0^{I0}$ | $I.8 \cdot I0^{I0}$ |
| | $B_{max}$ (км) | 7 700 | I0 700 | I2 950 |
| 60° | $N_\xi$ | 404 | 2 999 | 3 375 |
| | $Sh_I$ | $5.6 \cdot I0^{8}$ | $7.5 \cdot I0^{I0}$ | $I.5 \cdot I0^{I0}$ |
| | $B_{max}$ (км) | 7 750 | I0 650 | I2 250 |
| 90° | $N_\xi$ | 290 | 2 9I7 | 2 3II |
| | $Sh_I$ | $3.0 \cdot I0^{8}$ | $7.9 \cdot I0^{I0}$ | $I.I \cdot I0^{I0}$ |
| | $B_{max}$ (км) | 7 800 | I0 500 | II I00 |

filling of the UV plane and the data presented in table 1, make it possible to draw the following conclusions:

1. The filling of the plane of spatial frequencies by the RASSAS-1 system that consists of two radio telescopes (one ground-based and one space) is much higher than the filling done by the ground-based two-component intercontinental radio interferometers of the type VLBI.

2. Filling of the UV-plane by the RASSAS-1 system in 24 hours is significantly better (on the average) than the filling done by the multiple-antenna /26 (up to 10 antennas) global interferometric systems; here with an increase in the duration of observations over 24 h RASSAS-1 makes it possible to obtain even more complete filling, which, of course, is impossible in the VLBA system.

3. In the case of observance of a weak source for 24 h, the information content (according to Shennon) of RASSAS-1 on the average is three times inferior to the information content of VLBA (10 telescopes), which is evidently due to the considerable differences in the collection areas. It is easy to show that the indicated information content is compared for both systems with the 7-antenna

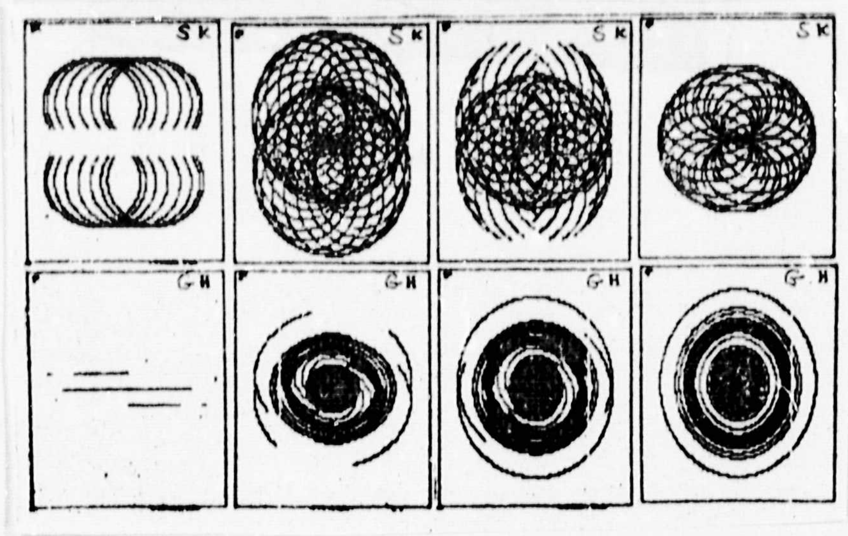


Figure 15. Charts for Filling UV-Plane in $T_H$=24 h by VLBA Systems (index "G" and RASSAS-1 (index "S") for Studied Objects with $\alpha=18^h$, $\delta=0°$ (1) 45° (2), 60° (3), 90° (4). Division of the UV-plane into 101 x 101 cells

VLBA variant. But such a system will fill already roughly three times fewer cells of the UV-plane as compared to RASSAS-1.

4. In the comparison of the time-linked observation program for the RASSAS type systems it is necessary to consider the direct ascent of the sources and the precession of the SRT orbital plane in order to obtain the optimal filling of the spectrum of spatial frequencies for each source included in the program.

5. The described algorithms and the programs of numerical modeling for the filling of the UV-plane by the RASSAS-1 system can be used to select objects for study and compilation of the time sequence of their observations in real experiments on a space radio interferometer.

References

1. Buyakas, V. I.; Gvamichava, A. S.; et al., Neogranichenno narashchivayemyy kosmicheskiy radioteleskop ["Unlimited-Accumulation Space Telescope"], Preprint of the Institute of Space Research, USSR Academy of Sciences, No 373, 1977.

2. Buyakas, V. I.; Gvamichava, A. S.; et al., Kosmicheskiye issledovaniya, 16 (1978), No. 5.

3. Powell, N. V.; Hibbs, A. R. Astron. Aeronaut, 15, No. 12 (1977), 58.

4. Basler, R. P.; Johnson, G. L.; and Vondrak, R. N. Radio Sci., 12, No. 5 (1977), 845.

5. Fomalont, E.; and Rayt, M. in Galakticheskaya i vnegalakticheskaya radioastronomiya ["Galactic and Extragalactic Radio Astronomy"], Moscow, Mir, 1976.

6. Yesepkina, N. A.; Korol'kov, D. V.; and Pariyskiy, Yu. N. Radioteleskopy i radiometry ["Radio Telescopes and Radiometry"], Moscow, Nauka, 1973.

7. Aksenov, Ye. P. Teoriya dvizheniya iskusstvennykh sputnikov Zemli ["Theory of the Movement of Artificial Earth Satellites"], Moscow, Nauka, 1977.

8. Hogbom, J. A. Astron. Astrophys., Suppl., 15 (1974), 417.

9. Wernecke, S. J., Radio Sci., 12, No. 5 (1977), 831.

10. Kellermann, K. I. VLBI Network Studies. III. An Intercontinental Very Long Baseline Array, NRAC Report, 1977.

11. Kogan, L. V. Sverzhdal'nyaya interferometriya kompaktnykh radioisotchnikov ["Ultra Long-Range Interferometry of Compact Radio Sources"], Candidate dissertation, Institute of Space Research, USSR Academy of Sciences, 1972.

Appendix. Program of Numerical Modeling of UV-Plane Filling by Radio Astronomical Space System of Aperture Synthesis

The program of numerical modeling of UV-plane filling by a radio astronomical space system of aperture synthesis consists of the main program (MAINPGM) and the subprograms ANGL, ORBII, MZERO, SCALE, BASIS, VPROD, STATB and OUTUV. /42

The MAINPGM implements the input and control opening of the constants and initial data, and gives the initial data in the necessary form. The initial data and the constants are introduced with the help of the operators DATA and appropriation. The constants are PI=3.14..., radius of the earth RE, acceleration of the gravity force on the earth's surface G, angular velocity of the earth's rotation WE. The initial data: PHI(1), PHI (2)--geographical latitude and longitude of the GRT; PSI (1), PSI(2), PSI(3), H--longitude of ascending angle of SRT orbit, incline of orbital plane, beginning phase at moment of time TO and height of orbit; ALF(1), ALF(2)--direct ascent and inclination of observed source; TO, T, DT--beginning of time reading, duration of observation, and spacing of quantization of process in time. All the distances are expressed in km, the time in min, the angles (except ALF(1)) in degrees, ALF(1)--in hours. During its work the MAINPGM generates the subprograms ANGL, ORBII, STATB and OUTUV.

The subprogram ANGL translates the angles from degree measures to radians. The input parameters: RAD--number of radians per degree, ANG--identifier of angle file subject to transformation, N--length of file. The output values for the angles are contained in the ANG file.

The subprogram ORBII strictly models the process of UV-plane filling by the RASSAS system. The input parameters: PI=3.14..., F--identifier of file, removed /43 for the UV-plane area to be filled, PSI, PHI, ALF--files of angular parameters of the system, N--size of the file F, NC--coordinates for the center on the UV-plane, RS, RE--radii of orbit and earth, RM--inverse size of one cell on the UV-plane, WS, WE--angular velocities of SRT and earth rotation, T, D, T--duration of observation and spacing of quantization with respect to time. After fulfillment of the subprogram, all the parameters except F remain unchanged, and the cells of the file F contain filling of the UV-plane, i.e., the time for stay of the projection for the system base vector in the given cell of the UV-plane. The generated subprograms: MZERO, SCALE, BASIS.

Subprogram MZERO brings to zero the two-dimensional file X of size N x N.

The subprogram-function SCALE makes a scalar product of two three-component vectors presented in the form of files A and B of length 3 cells.

The subprogram BASIS determines the basis on the UV-plane. The input parameters: PI=3.14..., ALF--file 2 cells long containing the source coordinates. The output parameters: A, BU, BV--files 3 cells long corresponding to the vector, direction to the studied object, and basis vectors on the UV-plane. The generated subprogram is VPROD.

The subprogram VPROD makes a vector product of two three-component vectors A and B. The result is arranged in the file C of length 3 cells.

The subprogram STATB statistically processes the results of UV-plane filling. The input parameters: F--file of cells of the UV-plane, N--its size, NC--coordinate of the center on the UV-plane, DR--size of one cell in km, T--duration of observation. During the operation of the subprogram the following amounts are determined and issued in print: N--number of filled cells, NO--number of cells /44
in circular region with radius equal to the maximum realized base, KF--coefficient of filling of circular region, BM--maximum realized base, XM and YM--maximum realized values for the base projections on the axis U and V, TMIN, TMAX, TEV--minimum, maximum and average time of accumulation for one cell, TUSE--"pure"synthesis time, KUSE--coefficient of use of the time in the given numerical experiment, AINF--information content of the synthesized aperture for a weak signal. In addition, the distribution function for the number of filled cells according to the accumulation time for one cell is determined and issued in print. An example of the output of the statistical characteristics is given below.

The subprogram OUTUV produces a display in print of the UV-plane filling in two gradations. The input parameters: F--identifier of derived two-dimensional file, N--its size.

The listings of the described subprograms are given below.

```
DOS/ES FORTRAN IV V.M 2.0                        MAINPGM              DATE

0001            DIMENSION F(101,101)
0002            DIMENSION ALF(2),PSI(3),PHI(2)
0003            DATA PI,RE/3.141592,6330.0/
0004            DATA G,WE/35.316,4.363322-3/
0005            DATA PHI/45.0,0.0/
0006            DATA PSI/0.0,52.0,0.0/
0007            DATA ALF/18.0,19.0/
0008        100 FORMAT(//2X,110(1H*),
               *//10X,'INITIAL DATA              ')
0009        110 FORMAT(/10X,'GRT COORDINATES      ',
               *2X,'PHI(1)=',F6.1,1X,'DEG',/,
               *26X,'PHI(2)=',F6.1,1X,'DEG  ')
0010        120 FORMAT(/10X,'PARAMETERS OF ORBIT     H',
               */26X,'PSI(1)=',F6.1,1X,'DEG  ',
               */26X,'PSI(2)=',F6.1,1X,'DEG  ',
               */26X,'PSI(3)=',F6.1,1X,'DEG  ')
0011        130 FORMAT(31X,'H=',F6.1,1X,'KM',
               */30X,'TS=',F6.1,1X,'MIN')
0012        140 FORMAT(/10X,'OB"EKT',12X,
               *'ALFA=',F6.2,1X,'HOUR',
               */27X,'DELTA=',F6.2,1X,'DEG  ')
0013        150 FORMAT(/10X,'EXPOSURE
               *11X,'T=',F7.1,1X,'MIN',
               */30X,'DT=',F7.1,1X,'MIN')
0014        160 FORMAT(/10X,'QUANTIZATION        UV-',
               *1X,'PLANE      ',/30X,'DR=',
               *F6.1,1X,'KM  ON CELL
0015        170 FORMAT(/10X,52(1H*))
0016            TO=0.0
0017            H=350.0
0018            T=1440.0
0019            DT=0.1
0020            N=101
0021            NC=51
0022            RS=RE+H
0023            WS=SQRT(G*RE**2/RS**3)
0024            TS=PI*2.0/WS
0025            RM=FLOAT(NC-1)/(RS*2.0)
0026            DR=1.0/RM
0027            PRINT 100
0028            PRINT 110,PHI
0029            PRINT 120,PSI
0030            PRINT 130,H,TS
0031            PRINT 140,ALF
0032            PRINT 150,T,DT
0033            PRINT 160,DR
0034            PRINT 170
0035            RAD=PI/180.0
0036            CALL ANGL(RAD,PHI,2)
0037            CALL ANGL(RAD,PSI,3)
0038            PHI(2)=PHI(2)+TO*WE
0039            CALL ORBIT
               *(PI,F,N,NC,PSI,PHI,ALF,RS,RE,RM,WS,WE,T,DT)
0040            CALL STATB(F,N,NC,DR,T)
0041            CALL OUTUV(F,N)
0042            STOP
0043            END
```

```
DOS/ES FORTRAN IV V.M 2.0                        ANGL                 DATE

0001            SUBROUTINE ANGL(RAD,ANG,N)
0002            DIMENSION ANG(N)
0003            DO 1 I=1,N
0004          1 ANG(I)=ANG(I)*RAD
0005            RETURN
0006            END
```

DOS/ES FORTRAN IV V.M 2.0 ORBI: DATE

```
      SUBROUTINE ORBI1
     *(PI,F,N,NC,PSI,PHI,ALF,RS,RE,RM,WS,WE,T,DT)
      DIMENSION F(N,N)
      DIMENSION ALF(2),PSI(3),PHI(2)
      DIMENSION A(3),BU(3),BV(3),XS(3),XE(3)
      CALL MZERO(F,N)
      CALL BASIS(PI,ALF,A,BU,BV)
      RE2=RE**2
      PS=PSI(3)
      PE=PHI(2)
      A1=RS*COS(PSI(1))
      A2=RS*SIN(PSI(1))
      B1=A2*COS(PSI(2))
      B2=A1*COS(PSI(2))
      B3=RS*SIN(PSI(2))
      C=RE*COS(PHI(  ))
      XE(3)=RE*SIN(PHI(1))
      DPS=WS*DT
      DPE=WE*DT
      NT=IFIX(T/DT)+1
      DO 4 I=1,NT
      PS=PS+DPS
      PE=PE+DPE
      XE(1)=C*COS(PE)
      XE(2)=C*SIN(PE)
      IF(SCAL3(XE,A)) 4,4,1
    1 CS=COS(PS)
      SS=SIN(PS)
      XS(1)=A1*CS-B1*SS
      XS(2)=A2*CS+B2*SS
      XS(3)=B3*SS
      BSU=SCAL3(XS,BU)
      BSV=SCAL3(XS,BV)
      IF(SCAL3(XS,A)) 2,2,3
    2 IF(BSU**2+BSV**2-RE2) 4,4,3
    3 BEU=SCAL3(XE,BU)
      BEV=SCAL3(XE,BV)
      K=IFIX((BSU-BEU)*RM)
      L=IFIX((BSV-BEV)*RM)
      K1=NC+K
      K2=NC-K
      L1=NC+L
      L2=NC-L
      F(K1,L1)=F(K1,L1)+DT
      F(K2,L2)=F(K2,L2)+DT
    4 CONTINUE
      RETURN
      END
```

DOS/ES FORTRAN IV V.M 2.0 MZERO DATE

```
      SUBROUTINE MZERO(X,N)
      DIMENSION X(N,N)
      DO 1 I=1,N
      DO 1 J=1,N
    1 X(I,J)=0.0
      RETURN
      END
```

DOS/ES FORTRAN IV V.M 2.0 SCAL3 DATE

```
      FUNCTION SCAL3(A,B)
      DIMENSION A(3),B(3)
      S=0.0
      DO 1 I=1,3
    1 S=S+A(I)*B(I)
      SCAL3=S
      RETURN
      END
```

DOS/ES FORTRAN IV V.M 2.0 BASIS DATE

```
      SUBROUTINE BASIS(PI,ALF,A,BU,BV)
      DIMENSION ALF(2)
      DIMENSION A(3),BU(3),BV(3)
      RAD=PI/180.0
      ALF(1)=ALF(1)/24.0*360.0*RAD
      ALF(2)=ALF(2)*RAD
      TET=PI/2.0-ALF(2)
      GAM=ALF(1)+PI
      A(1)=SIN(TET)*COS(ALF(1))
      A(2)=SIN(TET)*SIN(ALF(1))
      A(3)=COS(TET)
      BV(1)=SIN(ALF(2))*COS(GAM)
      BV(2)=SIN(ALF(2))*SIN(GAM)
      BV(3)=COS(ALF(2))
      CALL VPROD(BV,A,BU)
      RETURN
      END
```

DOS/ES FORTRAN IV V.M 2.0 VPROD DATE

```
      SUBROUTINE VPROD(A,B,C)
      DIMENSION A(3),B(3),C(3)
      C(1)=A(2)*B(3)-A(3)*B(2)
      C(2)=A(3)*B(1)-A(1)*B(3)
      C(3)=A(1)*B(2)-A(2)*B(1)
      RETURN
      END
```

DOS/ES FORTRAN IV V.M 2.0 STATS DATE

```
      SUBROUTINE STATS(F,N,NC,DR,T)
      DIMENSION F(N,N)
      DIMENSION IP(10),G(10)
  100 FORMAT(//10X,'STATISTICAL
     *1X,'CHARACTERISTICS
  110 FORMAT(/10X,'N =',I6,
     */10X,'NO=',I6,/10X,'KF=',F5.3,
     */10X,'DM=',F6.1,' (OF CELLS)
     *=',F7.1,'(KM)')
  115 FORMAT(/10X,'XM=',F4.1,1X,'OF CELLS'
     */10X,'YM=',F4.1,1X,'OF CELLS')
  120 FORMAT(/10X,'TMIN=',F8.1,1X,'SEC',
     */10X,'TEV =',F8.1,1X,' SEC
     */10X,'TMAX=',F8.1,1X,' SEC)
  125 FORMAT(/10X,'TUSE=',F8.1,1X,' MIN
     */10X,'KUSE=',F8.3)
  130 FORMAT(/10X,'INFORMATION CONTENT',
     *1X,'OF SYSTEM',/15X,'AINF=',
     *1X,ETC.4,1X,'(KM**2)*SQRT(SEC)')
  140 FORMAT(/10X,55(1H*))
  150 FORMAT(//10X,' DISTRIBUTION  ',
     *1X,' NUMBER   ',
     */10X,'OF FILLED CELLS
     */10X,'FOR TIME OF ACCUMULATION
  160 FORMAT(/10X,'T=',10F5.2,1X,'*TMAX')
  170 FORMAT(10X,'N=',10I5)
  180 FORMAT(10X,'G=',10F5.2)
      DM=0.0
      NP=0
      TEV=0.0
      TMAX=0.0
      AINF=0.0
      XM=0.0
      YM=0.0
      DO 4 I=1,N
      X=FLOAT(I-NC)
      DO 4 J=1,N
      Y=FLOAT(NC-J)
      IF(F(I,J)) 4,4,1
    1 NP=NP+1
      TEV=TEV+F(I,J)
      AINF=AINF+SQRT(F(I,J))
      XA=ABS(X)
      YA=ABS(Y)
      IF(XA.GT.XM)XM=XA
      IF(YA.GT.YM)YM=YA
```

```
      R=SQRT(X**2+Y**2)
      IF(R-BM) 3,3,2
    2 BM=R
      XB=X
      YB=Y
      TANB=Y/X
    3 IF(F(I,J).GT.TMAX)TMAX=F(I,J)
    4 CONTINUE
      TMIN=TMAX
      DO 6 I=1,N
      DO 6 J=1,N
      IF(F(I,J)) 6,6,5
    5 IF(F(I,J).LT.TMIN)TMIN=F(I,J)
    6 CONTINUE
      NO=IFIX(3.1415*BM**2)
      AKF=FLOAT(NP)/FLOAT(NO)
      TUSE=TEV/2.0
      AT=TUSE/T
      TEV=TEV/FLOAT(NP)*60.0
      TMAX=TMAX*60.0
      TMIN=TMIN*60.0
      BMM=BM*DR
      AINF=AINF*DR**2*SQRT(60.0)
      PRINT 100
      PRINT 110,NP,NO,AKF,BM,BMM
      PRINT 115,XM,YM
      PRINT 120,TMIN,TEV,TMAX
      PRINT 125,TUSE,AT
      PRINT 130,AINF
      PRINT 140
      AP=FLOAT(NP)
      TMS=600.0/TMAX+1.0
      DO 7 I=1,10
      IP(I)=0
    7 G(I)=FLOAT(I)*0.1
      PRINT 150
      PRINT 160,G
      DO 9 I=1,N
      DO 9 J=1,N
      IF(F(I,J)) 9,9,8
    8 K=IFIX(F(I,J)*TMS)+1
      IP(K)=IP(K)+1
    9 CONTINUE
      DO 10 I=1,10
   10 G(I)=FLOAT(IP(I))/AP
      PRINT 170,IP
      PRINT 180,G
      RETURN
      END
DOS/ES FORTRAN IV V.M 2.0                OUTUV                DATE
      SUBROUTINE OUTUV(P,N)
      DIMENSION F(N,N)
      DIMENSION P(103)
      DATA A,B,C,D/1HI,1H-,1H ,1H*/
   99 FORMAT(///)
  100 FORMAT(10X,103A1)
      PRINT 99
      NP1=N+1
      NP2=N+2
      NP3=N+3
      P(1)=A
      P(NP2)=A
      DO 1 I=1,NP1
    1 P(I)=B
      IF(NP3.GE.103)GOTO 3
      DO 2 I=NP3,103
    2 P(I)=C
    3 PRINT 100,P
      DO 7 J=1,N
      DO 6 I=1,N
      IF(F(I,J)) 4,4,5
    4 P(I+1)=C
      GO TO 6
    5 P(I+1)=D
    6 CONTINUE
    7 PRINT 100,P
      DO 8 I=2,NP1
    8 P(I)=B
      PRINT 100,P
      RETURN
      END
```

```
********************************************************************
INITIAL DATA
  CRT COORDINATES    PHI(1)=  45.0 DEG
                     PHI(2)=   0.0 DEG
  ORBIT PARAMETERS
                     PSI(1)=   0.0 DEG
                     PSI(2)=  52.0 DEG
                     PSI(3)=   0.0 DEG
                         H=  350.0 KM
                        T0=   91.2 MIN
  OBJECT               ALFA= 18.00 HOUR
                      DELTA= 15.00 DEG.
  EXPOSURE                 T= 1440.0 MIN
                          DT=    0.1 MIN
  QUANTIZATION OF UV-PLANE
                     DR= 267.2 KM ON CELL
**************************************************************

STATISTICAL CHARACTERISTICS
N =  2241
NO=  7128
KF=0.314
BM=47.6(CELLS) =12727.8(KM)
XM=61.0   CELLS
YM=30.0   CELLS
TMIN=     6.0  SEC
TEV =    38.9  SEC
TMAX=   312.0  SEC
TUSE=   670.4  MIN
KUSE=   0.466
INFORMATION CONTENT OF SYSTEM
    AINF=  0.9151E 09 (KM**2)*SQRT(SEC)
**************************************************************

DISTRIBUTION OF NUMBER OF FILLED
CELLS ACCORDING TO TIME
OF ACCUMULATION
T= 0.10 0.20 0.30 0.40 0.50 0.60 0.70 0.80 0.90 1.00 *TMAX
N=  522  934  602  100   48   18    2    8    0    0
G= 0.23 0.42 0.27 0.04 0.02 0.01 0.00 0.00 0.0  0.0
```

TABLE OF CONTENTS